



Original Article

Ag-decorated TiO₂ Nanofibers for Surface-enhanced Raman Scattering

Le Thi Ngoc Loan^{1,*}, Le Thi Thanh Hiep², Hoang Thi Hang¹, Le Xuan Hung²

¹Quy Nhon University, 170 An Duong Vuong, Nguyen Van Cu, Quy Nhon, Vietnam

²Duy Tan University, 254 Nguyen Van Linh, Thanh Khe, Da Nang, Vietnam

Received 15 May 2021

Revised 02 July 2021; Accepted 07 July 2021

Abstract: In this report, SERS substrates based on Ag-decorated TiO₂ nanofibers electrospun on a glass substrate (Ag/TiO₂/glass) were successfully prepared using electrospinning and photodeposition methods. XRD pattern demonstrated that the crystalline structure of TiO₂ nanofibers (TiO₂ NFs) consisted of both anatase and rutile phase. SEM images show that the randomly oriented on glass substrate TiO₂ NFs' diameters are in the range of 150 nm-300 nm and their lengths are up to a few micrometers. After 15-minute photodeposition, Ag NPs with average diameter of about a few tens of nanometers were uniformly and densely decorated on TiO₂ NFs surface. The Ag/TiO₂/glass SERS substrate was then immersed in 0.01 mM, 0.1 mM, and 1 mM 4-mercaptobenzoic acid (4-MBA) solution, and was afterwards investigated by UV-Vis absorption and Surface-enhanced Raman Scattering (SERS) spectra. The preliminary results show that the change in UV-Vis absorption corresponds well to the Raman peak intensity upon the adsorption of probed molecules. This might open up a pathway in the detection and identification of probed molecules based on colorimetric-sensing and SERS-sensing.

Keywords: Ag-decorated TiO₂, 4-MBA, Raman spectroscopy, SERS substrate

1. Introduction

Raman spectroscopy is an analytical technique that provides information about chemical structure, molecular interactions, and molecular conformations. Over the past decades, Raman spectroscopy has been used for various applications in materials science, and biomedical and chemical analysis. This technique provides information about molecular symmetry of small molecules and functional groups in

* Corresponding author.

E-mail address: lethingocloan@qnu.edu.vn

<https://doi.org/10.25073/2588-1124/vnumap.4649>

large and complex molecules, thus it is utilized for molecules detection and identification [1]. Since Raman scattering is a relatively weak process, several techniques have developed to improve Raman signals, including two popular techniques of the Surface-enhanced Raman Spectroscopy (SERS) and Tip-enhanced Raman Spectroscopy (TERS), where the later requires expensive equipment due to the combination of Raman spectroscopy with scanning probe microscopy.

Surface-enhanced Raman scattering was first experimentally observed by Fleischmann in 1974 when studying pyridine adsorbed on electrochemically roughened silver electrodes; however, the increase of Raman signals was attributed to an increased surface area [2]. In 1977, Jeanmarie and Van Duyne [3] observed a similar phenomenon and claimed that the increase of Raman intensity based on a new phenomenon. In 1978, Moskovitz attributed the increased scattering cross section to the excitation of surface plasmon on the rough silver surfaces [4]. Surface-enhanced Raman spectroscopy is an analytical technique based on plasmon-enhanced Raman scattering when molecules are located near metal surfaces. Over the past 45 years since its discovery, the SERS has been an important technique used in various fields such as biochemistry, biology, chemistry, and materials science. This technique not only includes all of the important attributes of Raman spectroscopy, i.e., providing molecular structural information or surface conformations of adsorbates on metal surfaces, but it is also very sensitive. Currently, there are two primary mechanisms that account for the SERS enhancement: i) Electromagnetic mechanism (EM) which requires the coupling of metallic nanoparticles and incident radiation [5]; and (ii) Chemical enhancement mechanism (CM) that contains a charge transfer (CT) process between substrate and adsorbates [6]. The dominant enhancement mechanism of SERS is the EM, which arises from the localized surface plasmon resonances (LSPR) effect created on nanostructured metal surface or metal nanogaps amongst nano-objects.

Traditionally, Au and Ag NPs suspensions have been widely used for the SERS technique due to enormous enhanced electromagnetic field (EF) generated on metal surface [7-9]. Furthermore, such noble metal suspension can be used for detection of molecules based on colorimetric sensing as they possess strong LSPR in the visible region, which is sensitive to the composition, size, shape, surrounding medium, aggregation state of these NPs and the refractive index of the surrounding environment [10, 11]. Hence, it is found that the SERS substrates based on Au NPs and Ag NPs exhibit high sensitivity or low detection limit [12]. In addition, the presence of metal nanoparticles on semiconductor substrates has recently attracted SERS due to the contribution of the CM mechanism accompanying the EM to the SERS signals [13]. Although Ag and Au both exhibit good plasmonic behavior in the visible range, Ag NPs have attracted great attention due to their cost-effectiveness compared to Au. Furthermore, TiO₂ semiconductor offers a good physical function and chemical stability; therefore, Ag-modified TiO₂ has been widely studied amongst SERS materials that made of metal/semiconductor nanocomposites. In terms of deposition of Ag NPs on TiO₂ surface, it was first synthesized and followed by photo deposition [14], chemical precipitation [15] and sputtering process [13]. In spite of the fact that numerous methods have reported to prepare Ag-modified TiO₂, a simple and cost-effective preparation method is still under seeking in the viewpoint of practical application. Here, we prepare SERS substrates based on TiO₂ nanofibers decorated with Ag NPs (Ag/TiO₂) by using electrospinning followed by photo deposition method. The substrates were used to explore the UV-Vis absorption and Raman spectra in the presence of 4-MBA as probed molecules at different concentrations. When the 4-MBA concentration changes, a change in the size and position of the LSPR peak in the UV-Vis spectrum is observable, which also corresponds well with the SERS measurements.

2. Experiment

2.1. Chemicals

All chemicals were purchased and utilized without further purification: poly(vinylpyrrolidone) (PVP) (wt. 360000, Sigma–Aldrich Co., Ltd), ethanol (C_2H_5OH , 99.8%), acetic acid (CH_3COOH , 99%), titanium tetraisopropoxide [$Ti(OiPr)_4$] 97%, Sigma-Aldrich Co., Ltd], distilled water (18.4 M Ω /cm), silver nitrate ($AgNO_3$; 0.1 M, Merck), 4-mercaptobenzoic acid powder (4-MBA, Sigma-Aldrich, analytical grade).

2.2. TiO_2 Nanofibers Preparation

The TiO_2 nanofibers (TiO_2 NFs) were synthesized employing electro-spinning method similar to the previous report [16]. Briefly, 0.4 grams of poly(vinylpyrrolidone) was dissolved in 8 mL of ethanol and stirred for 2 h. Next, 6 mL of titanium tetraisopropoxide and 4 mL of acetic acid were added to the as-prepared solution and stirred for 60 min at room temperature to obtain a sufficiently viscous solution for electro-spinning. The following step was to inject the precursor solution into a 5 mL syringe mounted on the syringe pump and fed into a metal needle. The precursor was then electro-spun by applying a high DC voltage of 10 kV across a distance of 12 cm toward the grounded collector. Noticeably, the precursor was constantly added by the syringe pump at a rate of 0.05 mL/h. A glass substrate (4 × 4 cm) was placed on the grounded collector for collection of nanofibers. After 4 hours of collection, the composite $Ti(OiPr)_4$ /PVP nanofibers on the glass substrate were collected and dried in ambient air for 3 h at 500 °C to form the TiO_2 NFs.

2.3. Ag NPs-modified TiO_2 NFs Surface

A photo-reduction method was used to deposit Ag nanoparticles on the surface of the TiO_2 NFs according to the previous work reported by F. Xu and co-workers [14]. 2 mL of aqueous silver nitrate solution (0.5 mM) and 0.04 g PVP was well-dispersed in 50 mL of ethanol in a 100 mL glass beaker to prepare the Ag^+ precursor. Then the as-prepared TiO_2 NFs on the glass substrates were immersed in the beaker, followed by irradiation with a UV lamp for 15 min to reduce Ag^+ to Ag^0 . Eventually, the substrates were washed in ethanol to remove the residuals and dried at 60 °C in atmosphere.

2.4. Characterizations

The morphology, crystalline structure of the samples were examined by field–emission scanning electron microscopy (FE–SEM; Hitachi S4800), X–ray diffraction (XRD, D8 Advance Eco, Bruker). The optical absorption spectra were obtained from the JASCO V-750 UV-Vis Spectrophotometer.

2.5. Raman characterization

The prepared Ag/TiO_2 /glass substrates were cleaned in oxygen plasma before being dipped in 4-MBA aqueous solution with different concentrations (0.01 mM, 0.1 mM and 1 mM) for 4 h. After that, the substrates were washed in ethanol to remove unfavorable molecules. Raman measurements were done using the XploRa Plus microscope, Horiba Jobin, laser 532 nm and integration time of 10 s.

3. Results and Discussion

3.1. Structural Analysis

X-ray diffraction (XRD) is a rapid analytical technique primarily used for phase identification of crystalline material. Figure 1 shows five typical diffraction angles of anatase phase of TiO_2 at 25.2°,

37.7°, 47.9°, 54.3, 75.1°, corresponding to diffraction planes (101), (004), (200), (211) and (215); and six peaks of rutile phase of TiO₂ at 27.4°, 36.5, 41.2°, 44.0°, 62.5° and 68.9°, representing the planes of (110), (101), (111), (210), (022) and ((301). These results indicate that the crystalline structure of the synthesized TiO₂ comprising of both anatase and rutile phase (according to the JCPDS card No. 84-1286 and No. 75-1753, respectively). The anatase phase found more dominant is evidenced by the intensity of the rutile peak (110) which was three times lower than the anatase one (101).

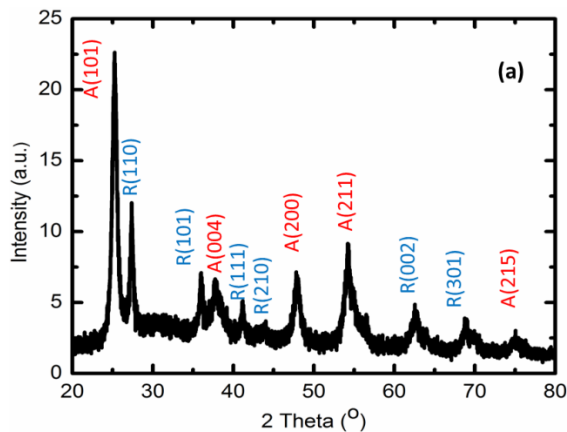


Figure 1. XRD pattern of the as-synthesized TiO₂ prepared by electrospinning method.

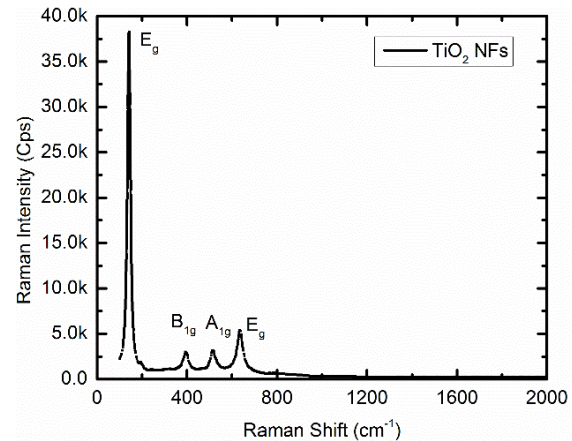


Figure 2. Raman spectrum of TiO₂ NFs shows four typical Raman active modes of anatase phase.

The composition and structure of the as-synthesized materials were further characterized by using Raman spectroscopy, a powerful and non-destructive method in order to study the chemical structure and phase of materials. According to the report of Frank [17], five vibration modes at Raman shift of 144 cm⁻¹ (E_g), 196 cm⁻¹ (E_g), 394 cm⁻¹ (B_{1g}), 516 cm⁻¹ (A_{1g}) and 638 cm⁻¹ (E_g) have been observed for typical TiO₂ anatase phase; while 4 Raman shifts at 145 cm⁻¹ (B_{1g}), 448 cm⁻¹ (E_g), 613 cm⁻¹ (A_{1g}), and 826 cm⁻¹ (B_{2g}) should be visible for rutile phase. Figure 2 demonstrates four vibrational peaks at 140 cm⁻¹, 395 cm⁻¹; 513 cm⁻¹, and 637 cm⁻¹ in the Raman spectrum of the as-synthesized TiO₂ in the range of 100 cm⁻¹ -1100 cm⁻¹, which corresponds to four Raman active modes of E_g, B_{1g}, A_{1g}, and E_g, respectively. The peak at 196 cm⁻¹ is absent in our measurements, and there is no Raman peak of the TiO₂ rutile phase can be found due to the dominance of the anatase phase as demonstrated in XRD characterization. These Raman characteristics show the dominant anatase phase of the as-synthesized TiO₂, which is in good agreement with the XRD pattern shown in Figure 1.

3.2. SEM Characterization

The morphologies of the as-prepared TiO₂ NFs and Ag-decorated TiO₂ (Ag/TiO₂) are characterized using Scanning Electron Microscope (SEM), shown in Figure 3. The TiO₂ NFs with diameters ranging from 150 nm to 300 nm, and the lengths were up to a few tens of micrometers, seen in Figure 3a; Figure 3b shows that the TiO₂ NFs were modified by Ag NPs, which were well-distributed on the surface of TiO₂ NFs with diameters of a few tens of nanometers after 15 min UV irradiation. The Ag NPs densely and uniformly distributed in all directions on the surface of TiO₂ NFs. The yellow arrows in the red box indicated the Ag NPs decorated on TiO₂.

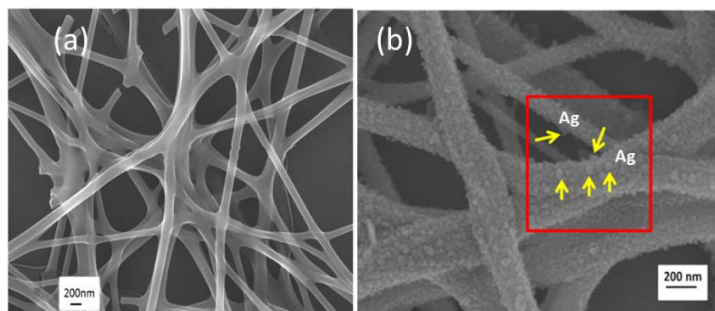


Figure 3. SEM image of the as-synthesized TiO₂ (a) and Ag NPs decorated the TiO₂ NFs surface (b).

3.3. UV-Vis Spectroscopy

Due to its large band gap, titanium dioxide nanofibers exhibit intrinsically strong absorption of ultraviolet (UV) light, seen in Figure 4a. Using Tauc method to determine optical band gap in semiconductor, the band gap of the as-synthesized TiO₂ NFs is approximately 3.15 eV; this is in good agreement with other reports [18, 19]. Figure 4b shows reflectance measurements of Ag/TiO₂/glass substrates before (black line) and after immersion in 4-MBA solution with concentration of 0.01 mM (pink line); 0.1 mM (blue line) and 1 mM (red line). Before immersion, the UV-Vis absorption spectrum of the bare Ag/TiO₂/glass shows a strong peak at 435 nm, accompanying the strong band gap absorption of the TiO₂ semiconductor in the ultraviolet region. This is attributed to surface plasmon resonance (SPR) effect generated on the surface of Ag NPs [20-22] and band to band transition, respectively. The change of color from white (TiO₂ NFs) to yellow-orange (Ag/TiO₂/glass) as seen in the inset pictures of Figure 4a and Figure 4b originated from the SPR effect [23]. After immersion of Ag/TiO₂/glass in 0.1 mM 4-MBA (0.1 mM 4-MBA/Ag/TiO₂) and 1 mM 4-MBA (1 mM 4-MBA/Ag/TiO₂) aqueous solution for 4 hours, 4-MBA molecules were attached to Ag NPs and TiO₂ NFs surface to form self-assembled monolayers (SAMs) [24]. This leads to a change in the semiconductor-insulator interface due to a replacement of air ($\epsilon=1$) by an organic layer with a different dielectric constant ϵ' . This results in a red-shift of the peak position and peak intensity for 0.1mM 4-MBA/Ag/TiO₂ (blue trace) and 1 mM 4-MBA/Ag/TiO₂ (red trace) samples in Figure 4b. In contrast, there is no change in the absorption peak position in the case of the Ag/TiO₂/glass immersed in 0.01 mM 4-MBA solution (0.01 mM 4-MBA/Ag/TiO₂); however, the absorption intensity is considerably damped (pink trace). This phenomenon illustrates that the 4-MBA molecules were already attached to Ag/TiO₂ surface although the molecular density was much less compared to the density of 4-MBA adsorbed on the surface of the 0.1 mM 4-MBA/Ag/TiO₂ and 1mM 4-MBA/Ag/TiO₂ samples. This observation will be further investigated by Raman measurements.

3.4. Raman Measurements

Figure 5 shows Raman signals of pure solid powder of 4-MBA in comparison with SERS signals of 4-MBA molecules adsorbed on TiO₂ NFs surface at different concentrations. Figure 5a shows normal Raman spectrum of 4-MBA powder, including active Raman vibrations at 216 cm⁻¹, 272 cm⁻¹, 340 cm⁻¹, 630 cm⁻¹, 803 cm⁻¹, 1096 cm⁻¹, 1180 cm⁻¹, 1290 cm⁻¹, 1593 cm⁻¹, and 1617 cm⁻¹. These vibration modes are in good agreement with previous reports [9, 25]. Figure 5b illustrates SERS spectrum of 1 mM 4-MBA self-assembled monolayers (SAMs) on Ag NPs. The inset of Figure 5b shows geometry model of the 4-MBA SAMs adsorbed on Ag NPs according to previous work [8, 9], implying that the adsorbed

4-MBA species may adopt a tilted orientation with respect to the silver surface. Compared to the Raman spectrum of 4-MBA powder, the number of Raman peaks is smaller for SERS spectrum, e.g., only four major peaks observed for SERS while ten Raman modes appeared in Raman spectrum. In addition, the intensity peak ratio between Raman and SERS spectra also changes, i.e. the intensity peak ratio between the characteristic ring-breathing modes $\nu(\text{CC})$ at 1074 cm^{-1} and 1574 cm^{-1} . Furthermore, an appearance of new strong peak at 1357 cm^{-1} in the SERS spectrum is assigned to the COO^- groups, which is resulted from direct interaction of the COO^- groups with the silver surface causing the titling of the molecular plane towards the metal surface [8]. The vibration band at 1174 cm^{-1} is associated to C-H bending vibration and observed in both Raman and SERS spectrum. The Raman bands of TiO_2 at 140 cm^{-1} (E_g), 395 cm^{-1} (B_{1g}), 513 cm^{-1} (A_{1g}), and 637 cm^{-1} (E_g) are significantly weaker than those of the pure TiO_2 NFs. More importantly, these low Raman-active range and enhanced Raman intensity make the $\text{Ag}/\text{TiO}_2/\text{glass}$ SERS substrates more accessible for detection of organic molecules, compared with other metal/oxide nanocomposites (i.e., $\text{Ag}/\text{Fe}_2\text{O}_3$).

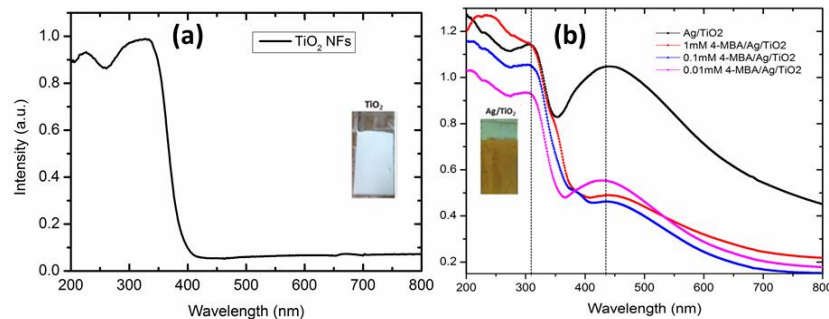


Figure 4. UV-Vis absorption spectra of TiO_2 NFs (4a) and $\text{Ag}/\text{TiO}_2/\text{glass}$ (black trace), $\text{Ag}/\text{TiO}_2/\text{glass}$ immersed in 4-MBA solution with concentration of 1 mM (red line); 0.1 mM (blue line) and 0.01 mM (pink line) (4b).

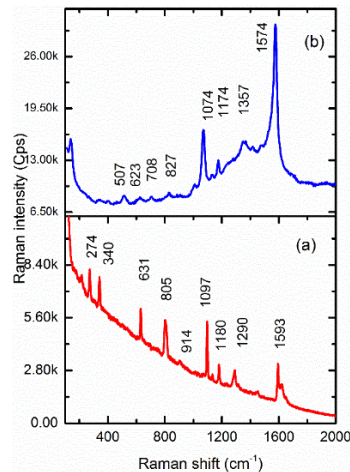


Figure 5. Comparison of Raman spectrum of pure 4-MBA powder (Figure 5a, red trace) and SERS spectrum of 1 mM 4-MBA/ Ag/TiO_2 (Figure 5b, blue trace).

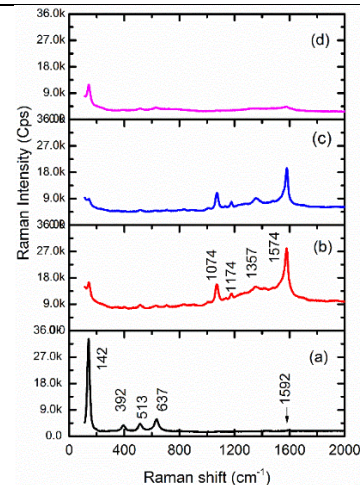


Figure 6. SERS spectra of 1 mM 4-MBA/ TiO_2 (Figure 6a, black trace), 1 mM 4-MBA/ Ag/TiO_2 (Figure 6b, red trace), 0.1 mM 4-MBA/ Ag/TiO_2 (Figure 6c, blue trace) and 0.01 mM 4-MBA/ Ag/TiO_2 (Figure. 6d, pink trace).

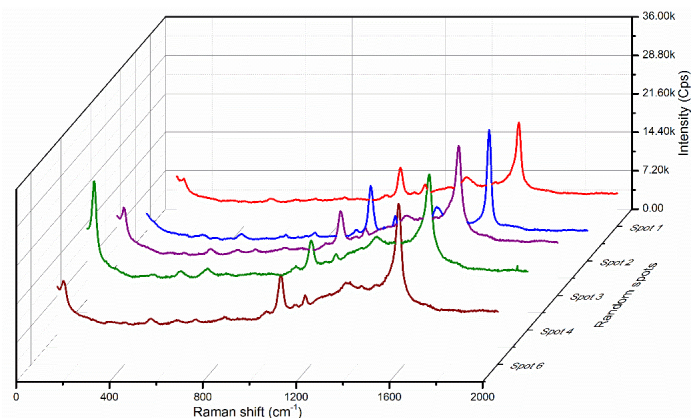


Figure 7. Raman spectra of 4-MBA obtained from five random spots on the Ag/TiO₂/glass SERS substrate.

Figure 6 shows the difference among Raman spectrum of 4-MBA ($C_m = 1$ mM) adsorbed to TiO₂ NFs (black trace) and SERS spectrum of 0.01 mM 4-MBA/Ag/TiO₂ (pink trace), 0.1 mM 4-MBA/Ag/TiO₂ (blue trace), and 1 mM 4-MBA/Ag/TiO₂ (red trace). There is only one small Raman peak of 4-MBA observed at 1592 cm⁻¹ in Figure 6a, while at least four dominant Raman peaks at 1074, 1174, 1357 and 1574 cm⁻¹ appeared in Figure 6b at the same concentration ($C_m = 1$ mM), which indicated an enhancement of SERS signals in the presence of Ag NPs. There is a blue-shift of the ring-breathing modes $\nu(\text{CC})$ in Figure 6b (1574 cm⁻¹) compared to itself in Figure 6a (1592 cm⁻¹) and Figure 5a (1593 cm⁻¹), which is associated to the binding sites and their orientation of 4-MBA molecules with respect to the Ag surface [9]. Furthermore, the Raman intensity of 4-MBA significantly decreased when the concentration of 4-MBA solution as seen in Figure. 6b ($C_m = 1$ mM), Figure 6c ($C_m = 0.1$ mM) and Figure 6d ($C_m = 0.01$ mM) decreased. This is because the Raman intensity proportional to the number of 4-MBA molecules adsorbed to the metal surface. This result is consistent with the observation in the UV-Vis spectra. Noticeably, the vibration band intensity of TiO₂ at 142, 392, 513 and 637 cm⁻¹ were significantly reduced for the sample 1 mM 4-MBA/Ag/TiO₂, 0.1 mM 4-MBA/Ag/TiO₂ and 0.001 mM 4-MBA/Ag/TiO₂ (Figure 6b-6d). Figure 7 illustrates SERS spectrum of 4-MBA at five random spots over 1 x 1 cm² Ag/TiO₂/glass SERS substrate. This demonstrates highly uniform SERS signals achieved over a large surface area (1 x 1 cm²).

The enhancement factor (EF) of the Ag/TiO₂ substrate can be estimated by the following equation:

$$EF = \frac{I_{SERS}/N_{SERS}}{I_{RS}/N_{RS}}, \quad (1)$$

where I_{SERS} and I_{RS} are the SERS and ordinary Raman intensities, respectively, which can be obtained experimentally [26]. We chose Gaussian function in Origin software to fit peaks and used the peak area of the strongest vibration peak at 1593 cm⁻¹ in both Raman and SERS spectrum (see Figures 5a and 5b) to obtain I_{SERS} and I_{RS} . N_{SERS} and N_{RS} are the numbers of molecules probed by SERS and ordinary Raman, in which N_{RS} is calculated by the number of probed molecules in the measurement volume or three-dimensional (3D) laser volume (V), while N_{SERS} is estimated by the number of 4-MBA molecules adsorbed on the surface of Ag/TiO₂ (n_{SC}). Approximately, we assumed that the 3D laser volume $V=1 \mu\text{m}^3$ (calibrated with Silicon peak at 520 cm⁻¹), molecular weight $MW_{4\text{-MBA}}=154.19$ g/mol, density $D_{4\text{-MBA}}=1.3$ g/cm and surface coverage density of thiol molecules $n_{SC}=0.71$ nM/cm² [27]. As a result, the estimated enhancement factor deduced from equation (1) $EF \sim 10^3$ for the as-prepared Ag/TiO₂, which can be further improved by Au NPs density and size, TiO₂ phase composition and shapes [28].

4. Conclusion

We have successfully prepared SERS substrates based on the Ag-decorated TiO₂ NFs on glass using electrospinning and photodeposition methods. The Ag NPs with sizes of a few tens of nanometers are densely and uniformly decorated on TiO₂ NFs, which resulted in high Raman signal enhancement due to the enhanced localized electromagnetic field. The change of substrate color from white (TiO₂ NFs) to yellow-orange (Ag/TiO₂/glass) is attributed to the appearance of the SPR effect generated on Ag NPs with the peak at 435 nm. The results of the UV-Vis absorption and the Raman spectra show that the Raman intensity decreases upon the decrease of 4-MBA density adsorbed to the Ag/TiO₂ surface, which is well-corresponding to UV-Vis absorption. Although the SERS enhancement primarily arises from the EM mechanism, further work is needed to demonstrate the impact of the charge transfer process between substrate and absorbate. The preliminary results indicate a strong correlation between the SPR and the SERS effect, which demonstrates that the as-prepared Ag/TiO₂/glass substrates can be an efficient substrate for sensitive molecules detection based on coloric- and Raman-sensing.

Acknowledgments

This study was conducted within the framework of science and technology projects at institutional level of Quy Nhon University under Project T2020.656.04.

References

- [1] J. R. Ferraro, K. Nakamoto, C. W. Brown, *Introductory Raman Spectroscopy*, Second ed., Elsevier, 2003
- [2] M. Fleischmann, P. J. Hendra, A. J. McQuillan, *Raman Spectra of Pyridine Adsorbed at a Silver Electrode*, *Chem. Phys. Lett.*, Vol. 26, No. 2, 1974, pp. 163-166.
- [3] D. L. Jeanmaire, R. P. V. Duyne, *Surface Raman Spectroelectrochemistry Part I, Heterocyclic, Aromatic, and Aliphatic Amines Adsorbed on the Anodized Silver Electrode*, *J. Electroanal. Chem.*, Vol. 84, 1977, pp. 1-20.
- [4] M. Moskovits, *Surface Roughness and the Enhanced Intensity of Raman Scattering by Molecules Adsorbed on Metals*, *J. Chem. Phys.*, Vol. 69, No. 9, 1978, pp. 4159.
- [5] M. Moskovits, U. Uerssi, *Surface-enhanced Spectroscopy*, *Rev. Mod. Phys.*, Vol. 57, No. 3, 1985, pp. 783-826.
- [6] A. Otto, *The Chemical (Electronic) Contribution to Surface-Enhanced Raman Scattering*, *J. Raman Spectrosc.*, Vol. 36, No. 6-7, 2005, pp. 497-509.
- [7] L. L. T. Ngoc, M. Jin, J. Wiedemair, A. V. D. Berg, E. T. Carlen, *Large Area Metal Nanowire Arrays with Tunable Sub-20 nm Nanogaps*, *ACS Nano*, Vol. 7, No. 6, 2013, pp. 5223-5234.
- [8] C. J. Orendorff, A. Gole, T. K. Sau, C. J. Murphy, *Surface-Enhanced Raman Spectroscopy of Self-Assembled Monolayers: Sandwich Architecture and Nanoparticle Shape Dependence*, *Anal. Chem.*, Vol. 77, No. 10, 2005, pp. 3261-3266.
- [9] A. Michota, J. Bukowska, *Surface-Enhanced Raman Scattering (SERS) of 4-Mercaptobenzoic Acid on Silver and Gold Substrates*, *J. Raman Spectrosc.*, Vol. 34, No. 1, 2003, pp. 21-25.
- [10] S. Chah, M. R. Hammond, R. N. Zare, *Gold Nanoparticles as a Colorimetric Sensor for Protein Conformational Changes*, *Chem. Biol.*, Vol. 12, No. 3, 2005, pp. 323-328.
- [11] H. Wei, S. M. H. Abtahi, P. J. Vikesland, *Plasmonic Colorimetric and SERS Sensors for Environmental Analysis*, *Environ. Sci. Nano*, Vol. 2, No. 2, 2015, pp. 12-135.
- [12] C. E. Talley, J. B. Jackson, C. Oubre, N. K. Grady, C. W. Hollars, S. M. Lane, T. R. Huser, P. Nordlander, N. J. Halas, *Surface-enhanced Raman Scattering from Individual Au Nanoparticles and Nanoparticle Dimer Substrates*, *Nano Lett.*, Vol. 5, No. 8, 2005, pp. 1569-1574.
- [13] Y. Wang, C. Yan, L. Chen, Y. Zhang, J. Yang, *Controllable Charge Transfer in Ag-TiO₂ Composite Structure for SERS Application*, *Nanomaterials*, Vol. 7, No. 7, 2017, pp. 1-11.

- [14] F. Xu, J. Mei, M. Zheng, D. Bai, D. Wu, Z. Gao, K. Jiang, Au Nanoparticles Modified Branched TiO₂ Nanorod Array Arranged with Ultrathin Nanorods for Enhanced Photoelectrochemical Water Splitting, *J. Alloys Compd.*, Vol. 693, 2017, pp. 1124-1132.
- [15] J. Singh, N. Tripathi, S. Mohapatra, Synthesis of Ag–TiO₂ Hybrid Nanoparticles with Enhanced Photocatalytic Activity by a Facile wet Chemical Method, *Nano-Structures and Nano-Objects*, Vol. 18, 2019, pp. 100266.
- [16] N. V. Nguyen, M. V. Nguyen, T. H. T. Nguyen, M. T. Doan, L. L. T. Ngoc, E. Janssens, A. Yadav, P. C. Lin, M. S. Nguyen, N. H. Hoang, Surface-Modified Titanium Dioxide Nanofibers with Gold Nanoparticles for Enhanced Photoelectrochemical Water Splitting, *Catalysts*, Vol. 10, No. 2, 2020, pp. 1-11.
- [17] O. Frank, M. Zúkalová, B. Lasková, J. Kürti, J. Koltai, L. Kavan, Raman Spectra of Titanium Dioxide (Anatase, Rutile) with Identified Oxygen Isotopes (16, 17, 18), *Phys. Chem. Chem. Phys.*, Vol. 14, No. 42, 2012, pp. 14567-14572.
- [18] V. N. Nguyen, M. T. Doan, M. V. Nguyen, Photoelectrochemical Water Splitting Properties of CdS/TiO₂ Nanofibers-based Photoanode, *J. Mater. Sci. Mater. Electron.*, Vol. 30, No. 1, 2019, pp. 926-932.
- [19] T. T. L. Le, L. T. Nguyen, H. H. Nguyen, V. N. Nguyen, M. V. Nguyen, N. H. Hoang, V. T. Nguyen, V. T. Le, V. H. Nguyen, P. C. Lin, A. Yadav, I. Madarevic, E. Janssens, H. V. Bui, L. L. T. Ngoc, Titanium Nitride Nanodonuts Synthesized from Natural Ilmenite Ore as a Novel and Efficient Thermoplasmonic Material, *Nanomaterials*, Vol. 11, No. 1, 2021, pp. 76-87.
- [20] S. Liu, G. Chen, P. N. Prasad, M. T. Swihart, Synthesis of Monodisperse Au, Ag, and Au-Ag Alloy Nanoparticles with Tunable Size and Surface Plasmon Resonance Frequency, *Chem. Mater.*, Vol. 23, 2011, pp. 4098-4101.
- [21] G. Schider, J. R. Krenn, W. Gotschy, B. Lamprecht, H. Ditlbacher, A. Leitner, F. R. Aussenegg, Optical Properties of Ag and Au Nanowire Gratings, *J. Appl. Phys.*, Vol. 90, No. 8, 2001, pp. 3825.
- [22] E. Hutter, J. H. Fendler, D. Roy, Surface Plasmon Resonance Studies of Gold and Silver Nanoparticles Linked to Gold and Silver Substrates by 2-Aminoethanethiol and 1,6-Hexanedithiol, *J. Phys. Chem. B*, Vol. 105, 2001, pp. 11159-11168.
- [23] W. Li, P. H. C. Camargo, X. Lu, Y. Xia, Dimers of Silver Nanospheres: Facile Synthesis and Their Use as hot Spots for Surface-enhanced Raman Scattering, *Nano Lett.*, Vol. 9, No. 1, 2009, pp. 485-490.
- [24] C. E. Taylor, J. E. Pemberton, G. G. Goodman, M. H. Schoenfish, Surface Enhancement Factors for Ag and Au Surfaces Relative to Pt Surfaces for Monolayers of Thiophenol, *Appl. Spectrosc.*, Vol. 53, No. 10, 1999, pp. 1212-1221.
- [25] H. Park, S. B. Lee, K. Kim, M. S. Kim, Surface-enhanced Raman Scattering of P-aminobenzoic Acid at Ag Electrode, *J. Phys. Chem.*, Vol. 94, No. 19, 1990, pp. 7576-7580.
- [26] A. I. P. Jiménez, D. Lyu, Z. Lu, G. Liu, B. Ren, Surface-enhanced Raman Spectroscopy: Benefits, Trade-offs and Future Developments, *Chem. Sci.*, Vol. 11, No. 18, 2020, pp. 4563-4577.
- [27] L. J. Wan, M. Terashima, H. Noda, M. Osawa, Molecular Orientation and Ordered Structure of Benzenethiol Adsorbed on Gold(111), *J. Phys. Chem. B*, Vol. 104, No. 15, 2000, pp. 3563-3569.
- [28] Y. Liu, H. Ma, X. X. Han, B. Zhao, Metal-semiconductor Heterostructures for Surface-enhanced Raman Scattering: Synergistic Contribution of Plasmons and Charge Transfer, *Mater. Horizons*, Vol. 8, No. 2, 2021, pp. 370-382.